Watershed transformation of time series of medical thermal images

Dietrich Paulus[a], Torsten Greiner[b], Christian L. Knüvener[a]
Lehrstuhl für Mustererkennung (Informatik 5)[a]
and
Institut für Physiologie und Experimentelle Pathophysiologie[b]
Friedrich–Alexander–Universität Erlangen–Nürnberg

paulus@informatik.uni-erlangen.de
greiner@ipb.uni-erlangen.de

To be printed in
Proceedings

SPIE Conf. on Intelligent Robots and Computer Vision XIV: Algorithms, Techniques, Active Vision, and Materials Handling

where/when
(12 pages)
Presentation 26–Oct–95
Number 2588–79

Inhaltsverzeichnis

Watershed transformation of time series of medical thermal images

Dietrich Paulus[a], Torsten Greiner[b]*, Christian L. Knüvener[a]
Lehrstuhl für Mustererkennung (Informatik 5)[a]
and
Institut für Physiologie und Experimentelle Pathophysiologie[b]
Friedrich–Alexander–Universität Erlangen–Nürnberg

paulus@informatik.uni-erlangen.de
greiner@ipb.uni-erlangen.de

ABSTRACT

In this paper, we demonstrate how the watershed transform can be applied to series of thermal medical images to compute important features for physiological interpretation. Automatic physiological analysis of neural features can thereby be shown which was not possible otherwise.

The transform as described in the literature has some minor algorithmic errors and inconsistencies which usually cause little trouble. These problems occur on flat plateaus where no unique watershed can be detected. After a short formal description of the transform we describe and eliminate these deficiencies and introduce a modified segmentation method which handles these plateaus as expected intuitively. In our particular medical application, visible differences of the new segmentation with respect to the old one can be noticed.

We contrast our results to those obtained by the detection of isothermic regions.

Features of the segmented regions are evaluated as a function of time and used for medical and physiological interpretation. An outlook describes current research in sensor fusion of visual and thermal images for medical research.

Keywords: image processing, segmentation, watershed transformation, C++, thermography, axon–reflex, vasodilatation, pain

1 INTRODUCTION

To investigate the mechanisms of pain origin and pain processing, experiments are carried out which are able to change the skin blood flow and therefore the temperature of the skin. This reaction is recorded by an infrared thermography camera. The resulting thermograms are the basis for further analysis by the medical observer.

After application of noxious stimuli to the skin a spreading vasodilatation can be observed. This leads in a visible reddening of the skin (the so called "flare"). This reaction is mainly based on the axon reflex mechanism which was first mentioned by Bruce[3] and Lewis.[13] The latter stated the releasing theory of a neurotransmitter which acts on small blood vessels. According to the studies of Bruce and Lewis the area of the resulting flare is determined by the anatomical arrangement of the collateral nerve network in the skin. The nerves involved in the vascular reflex are polymodal afferent nociceptive C–fibers.[4] To induce the local warming reaction noxious stimuli (intra-cutaneous histamine injection 10 μl, 0.1 %) were applied to the skin of the volar forearm of several healthy subjects aged 30–45. All subjects gave their informed consent and the study has been approved by the local ethics committee. To analyze the ongoing of the reaction series of thermal images were taken using an AGEMA 870 infrared camera system. Recordings were transferred to a PC via an interface (IR–SAVE, Gesotec, Germany). Images were taken every 200 ms (5 Hz). The resolution of the resulting digital image was 8 bit. The thermal resolution of the system was $0.1°C$, the spatial resolution of the thermograms was 128×155 pixels. To reduce noise, 50 frames have been averaged to one image. This results in a stored image sequence of 0.1 Hz.

We apply a segmentation method which emphasizes zones of higher reaction in the skin automatically. After a study of possible segmentation methods for thermal images (Sect. 2), we shortly introduce the watershed transform (Sect. 3) and present some modifications and enhancements (Sect. 4). Series of thermograms are processed to

*Supported by: Sonderforschungsbereich „Pathobiologie der Schmerzentstehung und Schmerzverarbeitung“ (SFB 353)

quantify the ongoing of the inflammation (Sect. 5). Due to this procedure, objective results for the physiological reaction can be presented (Sect. 6). The contribution closes with remarks on the implementation and an outlook on further research (Sect. 7).

2 SEGMENTATION OF THERMAL IMAGES

Segmentation of medical images is done to detect anatomic structures or phenomena. The main purpose is to better understand the anatomic relationships of the various objects. The objects to be found in thermal images are regions of similar temperature induced by local artificial inflammation. For this reason, the segmentation of thermal images is the distinction between inflamed and non–inflamed areas. Conventional methods like edge and line detection fail, even if problem specific preprocessing is applied, as can be seen in Figure 1.

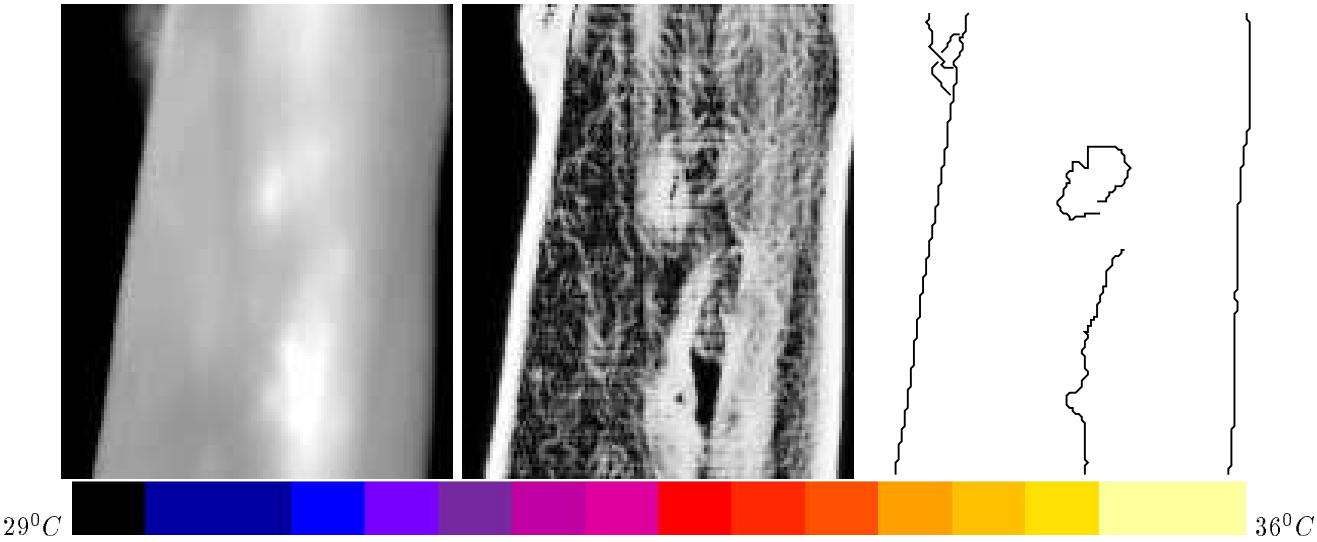

Figure 1: Thermographic image (left), edge strength computed with Shen edge detection[23] after contrast enhancement (middle), and line detection with hysteresis thresholds[10] (right).

One method to subdivide an image into inflamed and non–inflamed areas is to define a temperature threshold. We binarize the input image using this threshold, compute the contours of the binary regions, and call these lines the *isothermogram*. Figure 2 shows three examples of an isothermic representation processed on the same image. The disadvantage of this method is that the isothermic representation obviously depends on the threshold of the isothermic level. In Figure 2, the level chosen in the middle seems to be the best choice. A lower level (left) surrounds local maxima whereas a higher one (right) misses the lower temperature zones. The threshold for the inflammation is computed by analysis of the images captured before application ("baseline").

The watershed transform which will be introduced in Sect. 3 is another type of segmentation which turns out to be less sensitive to parameter changes of the threshold.

The aim of the watershed transform is to subdivide an image according to the occurred local minima. Therefore we used this segmentation technique for further image processing. A comparison of the segmentation results of a thermogram with two different methods is depicted in Figure 2 and Figure 3 (left). The latter clearly detects the local maxima whilst the result of the isothermic operation mainly depends on the level chosen for the isotherm (Figure 2).

In early implementations the watershed transformation took a lot of time to process an image because of the inefficient implementation. Vincent developed a new type of algorithm[24] and showed that the watershed transformation can be accelerated. The watershed transform was successfully applied for the segmentation of

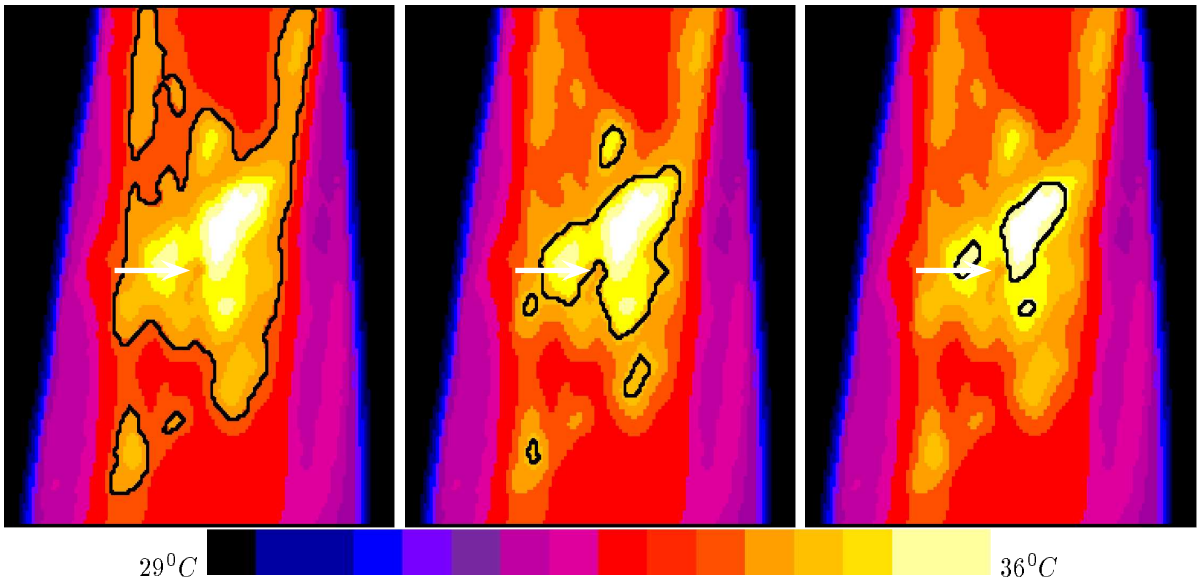

Figure 2: Isothermes (left 33.9^0C, middle 34.6^0C, right 35.3^0C). The arrow marks the injection site.

thermal images.[12,19,8] Other medical applications were segmented by Zehetbauer[27] using this transform.

3 WATERSHED TRANSFORMATION

The watershed transform according to Vincent[24] segments an image using image morphology. Watersheds separate adjacent water basins (Figure 3 (right)). The watershed transform idea can be easily explained by additional help of a geographical imagination. Suppose a drop of water is falling on a topographic relief — it will run down until it reaches a local minimum. The influence zones of those local minima are called catchment basins. As the water level increases and two basins are going to flow together, a dam has to be build. The dam separates the local minima against each other without any regards to certain thresholds. To use this algorithm for thermal image segmentation with respect to their local *maxima*, we have to invert the thermogram.

Several technical realizations of the watershed idea can be found in the literature and are summarized in Zehetbauer.[26] Digital elevation models are analyzed with different methods. These approaches are compared in Vincent.[24] Zehetbauer[24,26] discusses the algorithms by Digabel and Lantuéjoul,[5] Meyer and Beucher[2,14] and Friedlander.[7] Since Vincent[24] published his fast implementation, attention to this transformation has grown and very efficient realizations have been made in different areas, e.g. in Hanson & Higgins,[9] Dobrin et al.,[6] and in Saarinen.[22] Hanson uses edge images as input and interactively initializes a region segmentation process; edge images from color are segmented by Saarinen.[22] Both approaches mention the typical over–segmentation of this algorithmic approach. In Sect. 3, we extend the notion of Vincent for an advanced segmentation of gray level images which in our application avoids over–segmentation.

The two general ideas for the watershed transform are the *global* and the *local approach* to watershed segmentation. In the local approach, decision about further flow of water is based on the neighborhood of a pixel. In the global approach, all pixels are affected by the flooding. First (figuratively spoken) we are putting wholes into each local minimum. Now the mountains are immersed into water, which passes through the prepared holes. Whenever two basins unite, a dam is build (Figure 3 (right)). The computed contour lines of these dams surround the areas searched for. Dams are just another name for watersheds. During the flooding process, only the points on the boarder of the basin are required for computation. This contour based algorithm allows for an efficient

implementation when these points are queued and inspected in parallel.[24]

The immersion can be stopped at a certain level or can be continued until the highest mountain is covered by water and only dams remain visible. Partial flooding can be used to separate objects from the background (Figure 4).

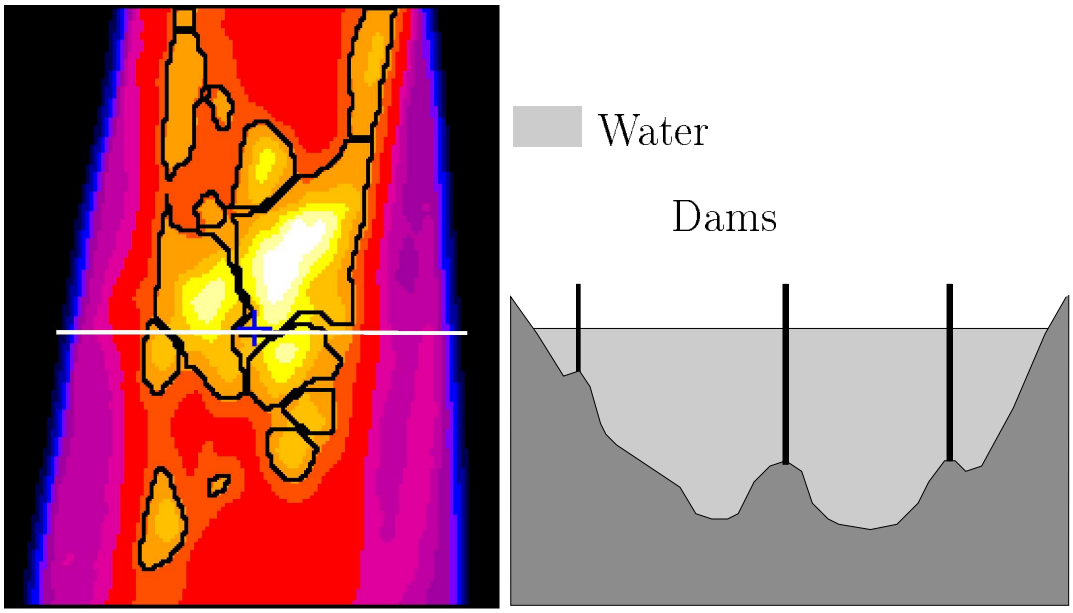

Figure 3: One–dimensional effect of the immersion simulation on a gray level profile (right) cut from a real thermographic image (white line on the left), modified method according to Baxes.[1] Immersion depth 33.9^0C.

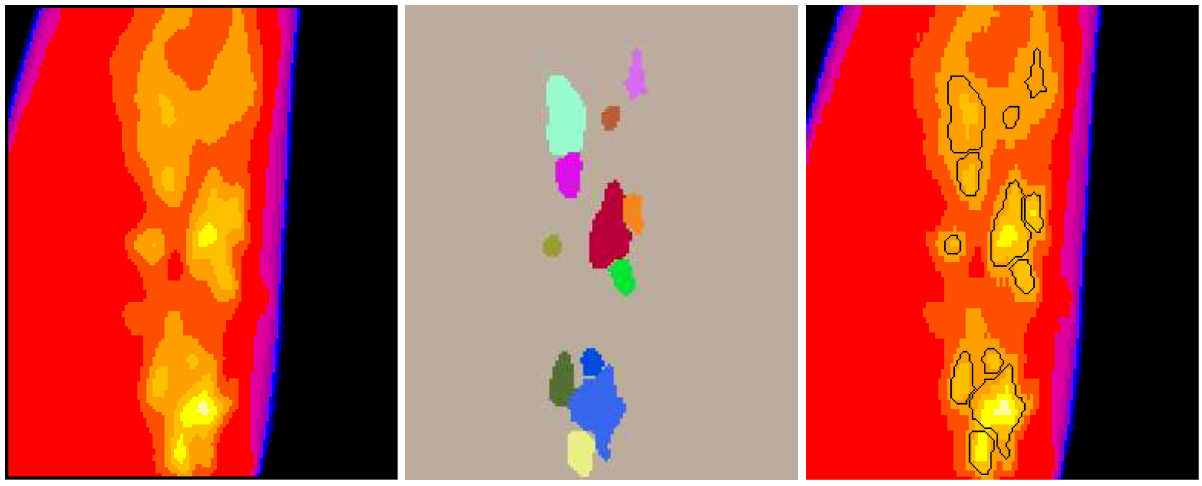

Figure 4: To separate objects from the background, the watershed transform algorithm stops after a certain level. thermographic image (left), label image (middle), contours (right). Immersion depth 33.08^0C.

Vincent[24] describes the watershed transform as a special case of a morphological operation. For segmentation purposes, the watershed transform can be treated as a region growing algorithm. Region segmentation requires

the definition of a criterion for homogeneity.[16] Catchment basins are homogeneous in the sense that they contain exactly one local minimum together with the related influence zone.

Using the global approach, the transformation of a 2D intensity image I to objects $C_{h_{max}}(M)$ and background $I-(\sum_M C_{h_{max}}(M))$ can be formulated: objects $C_{h_{max}}(M)$ mean the catchment basin of the local minimum M under flooding level h_{max}. Background is defined by the area which does not belong to any object (Figure 4).

When the topographical relief is flooded step by step, three basic situations can be observed:

1. A new object is registered if the water reaches a new local minimum. This pixel location is tagged with a new region label.
2. If a basin extends without uniting with another, the new borders have to be assigned to this basin.
3. If two basins are about to unite, a dam has to be built in between.

The critical point of the algorithm is how the dam will be set up. If we imagine a heavy rain falling on the relief, we expect a drop of water to flow to the next lower location whereby it will never flow uphill. The problem is to find the length of the path to the nearest location on the digital grid which is lower than the point where the rain drops on the terrain. The natural measure would be the use of the Euclidean distance; this is however computationally too expensive, especially if the line is long and curved. Vincent[24] uses the city–block distance in his formal description. In his formalism many points can not be assigned to a region because of this distance measure.

A better approach is to define a temporal process for a rain drop hitting the ground in a start location. A rain drop flows from one discrete location to its neighbor within one unit of time. The location is assigned to the region which is first reached by the possible flow of the drop.

Vincent defines the geodesic influence zone of a local minimum M. Let Y be a compound region consisting of compound subregions B_i. The geodesic influence $E_Y(B_i)$ is defined as the set of those pixels q in Y whose distance d_Y to any other component B_j in Y is greater than its distance to B_i. We use the eight neighbors of the actual point for the computation of the distance which is measured as the path length to the lake which must never run uphill. We now extend Vincent's notion of geodesic influence zones by the temporal process. The term $E_Y(C_h(M),t)$ is assigned to the zone belonging to the catchment basin $C_h(M)$ at time t and flooding level $h+1$. The local minimum with label a is denoted by M_a.

$$E_Y(C_h(M), t=0) = C_h(M) \tag{1}$$

$$E_Y(C_h(M_a), t+1) = E_Y(C_h(M_a), t) \cup \{q \in Y | \forall_{b \neq a} d_Y(q, C_h(M_a), t) = 1 < d_Y(q, C_h(M_b), t)\} \tag{2}$$

$$E_Y(C_h(M)) = \lim_{t \to \infty} E_Y(C_h(M), t) \tag{3}$$

When all pixels of a certain height h are flooded, the water level is increased by one. For a minimum of height h_0, the following equations hold:

$$C_{h<h_0}(M) = \emptyset \tag{4}$$

$$C_{h=h_0}(M) = M \tag{5}$$

$$C_{h+1>h_0}(M) = C_h(M) \cup E_Y(C_h(M)) \tag{6}$$

This approach is however still not sufficient, as can be seen later in Figure 9 (left). Up to now, the actual pixel which is reached during flooding is assigned to a watershed if those of its neighbors which were already processed, belong to different regions. This definition causes problems on flat surfaces.

The new probability algorithm[12] avoids those problems: In the neighborhood of the actual pixel all locations already processed are inspected and the number of pixels assigned to a region are counted. A probability is assigned to each region in the neighborhood based on the number of pixels assigned. The new pixel is added to the region which has the highest probability, as long as this value exceeds a parameter p_m to the algorithm. This parameter may vary between 51% and 100%. This is exemplified in Figure 5.

This new idea for the computation of the path can be expressed formally as a redefinition of (2).

$$E_Y(C_h(M_a), t+1) = E_Y(C_h(M_a), t) \cup \{q \in Y | \forall b : \sum_r \{d_Y(r, C_h(M_a), t) = 1\} \geq p_m \sum_r \{d_Y(r, C_h(M_b), t) = 1\}\} \tag{7}$$

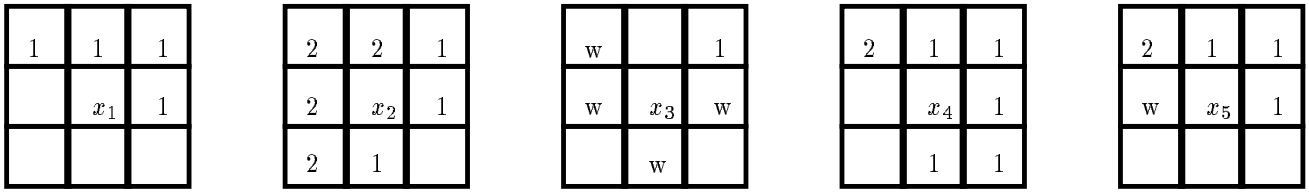

	x_1	x_2	x_3	x_4	x_5
Original algorithm	1	w	1	w	w
$p_m = 100\%$	1	w	w	w	w
$p_m = 67\%$	1	w	w	1	w
$p_m = 51\%$	1	2	w	1	1

Figure 5: Comparison of algorithms and parameters; the numbers denote region labels, w is a watershed.

4 ENHANCED watershed ALGORITHM

The original algorithm by Vincent is shown as a structogram here in Figure 6. The central idea for an efficient realization results from two facts. First, the pixels are sorted according to their intensity. Second, only those pixels are inspected during one iteration of flooding with water level h (see ** in Figure 6) which have already flooded neighbors; only those positions can be reached by water during this step.

Read input image
Sort pixel coordinates according to gray level
Initialize region image with label w
FOR all water levels from h_{min} to h_{max}:
Flood pixels of actual level which have already flooded neighbors **
If required, set up new region at new local minimum
UNTIL all pixels of actual level are flooded
Save resulting region image

Figure 6: Watershed algorithm according to Vincent.[24]

For an algorithmic solution of the enhanced watershed transform algorithm described above, pixels in the label image are assigned status attributes to mark whether a pixel has to be inspected during this flooding level ("marked"), is queued for further inspection ("queued"), or is finally assigned to a region or watershed ("done"). Initially, all pixels are initialized ("in it"). Vincent uses more status attributes, but these four have been found sufficient for the implementation. These attributes guarantee that pixels processed in the inner loop (*** in Figure 7) have no influence on each other; only already flooded pixels affect the assignment of a pixel to a region or watershed. The new algorithm is shown in Figure 7. The process of assigning a label to a pixel (++ in Figure 7) is shown in Figure 8.

The original algorithm creates a watershed which is completely surrounded by one region, rather than a watershed which limits the basin to its surrounding territory. In our application, this is not desired; our new extended algorithm does not show such behavior, as can be seen in Figure 9 (middle and right). In addition, the new algorithm yields smooth contours. An example of this further enhancement can be seen in Figure 10, middle.

Read gray level image			
Sort pixel coordinates according to gray level			
Initialize region image with label "watershed"			
Initialize status image with label „INIT"			
FOR all levels from h_{min} to h_{max}:			
	Mark all pixels of actual level (status: „MARKED")		
	Queue marked pixels with already marked neighbors (Status: „QUEUED")		
		Remember end of actual queue	
		Process pixel in queue and add marked neighbors to queue	++
		Delete mark for this pixel (Status: „DONE")	
	UNTIL End of actual queue		
	IF	There is still a marked pixel	
	THEN	Assign new label to pixel in region image	
		Delete mark for pixel (Status: „DONE")	
		Queue marked neighbor pixels (Status: „QUEUED")	
	UNTIL all pixels processed (queue empty)		***
Store region image			

Figure 7: Watershed algorithm with status attributes.

Count neighbor pixels marked "done" $\rightarrow n$ and count occurrences of labels		
FOR all such labels l		
	IF	$l \geq p_m * n$
	THEN label actual pixel with l	

Figure 8: Label assignment to a certain pixel.

5 Application to time series of thermal images

In this section we use the watershed transform to process time series of thermal images. To investigate histamine effects recordings are performed 2 min. before (baseline) and 15 min. after histamine application (approx. 120 images).

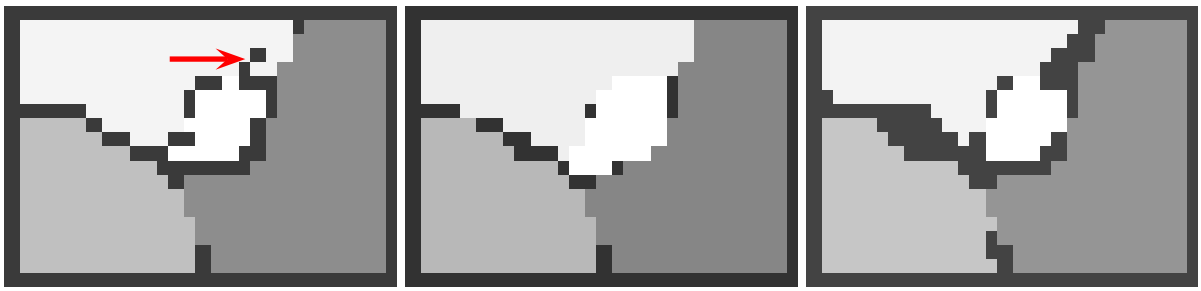

Figure 9: Section of a thermographic image. Vincent– (left), $p_m = 51\%$ (middle) and $p_m = 67\%$ (right). Black lines mark detected watersheds. The arrow marks the mentioned problem of the original algorithm.

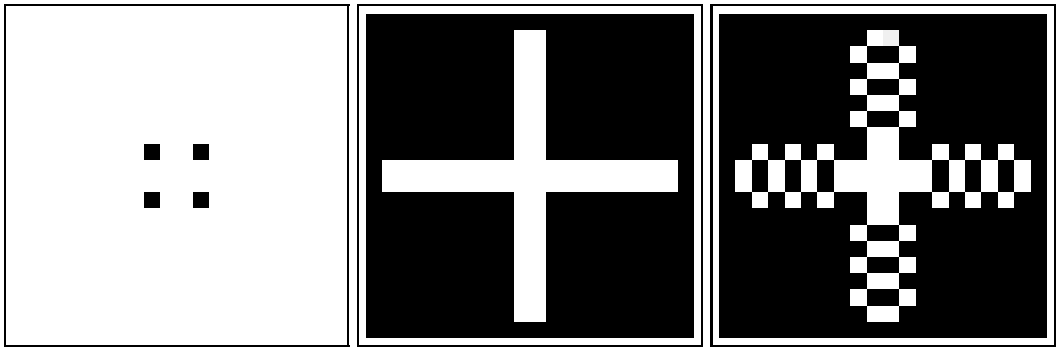

Figure 10: Test image (left), $p_m = 51$ % (middle) and original algorithm (right). Watersheds are drawn as white lines, boarders are regarded as background.

To quantify the spatial development of the reaction each image is processed in the following manner: First, a noise reduction using a 3×3 low pass filter is done. Then, each image is inverted because — as mentioned in Sect. 3 — the watershed transform usually subdivides an image according to the occurred local minima, but in this case local maxima detection is required. In the third step the maximum immersion depth (MID $= \mu + 2 * \sigma$, μ: mean, σ: standard deviation of an image without background) has to be evaluated. For this purpose we use some images from the baseline (before the stimulus is set). Now the watershed transformation can be carried out. Afterwards a contour detection algorithm[15] is used to evaluate the boundaries of the catchment basins. To interpret the results the contour must be visualized to the medical observer and at last a region feature detection and computation algorithm has to be used for quantitative analysis.

For quantitative analysis of the inflammation we computed the following features for each region: size (number of pixels), contour length (in pixels), temperature minimum, temperature maximum, center of gravity, mean temperature, and standard deviation. These values are the base for the graphical visualization.

6 RESULTS AND INTERPRETATION

An intracutaneous histamine injection evokes the cutaionous vascular axon reflex which results in a local warming reaction of the skin. The ongoing of this reaction mainly depends on the increased blood flow. Thermographic recordings revealed that the warming reaction usually started from distinct spots. The average distance was about 5-30 mm from the site where a small amount of histamine solution had been injected.

In Figure 11 three images out of a time series are shown. The objects have been detected by the modified watershed transform. The watershed boundaries split the image without any error in a way an experienced medical user would do this.

The time course of the temperature increase at individual spots depends on the distance of the injection site. A mathematical model for these curves can be described as a simple differential equation for the temperature T with a final temperature of T_R:

$$\frac{dT}{dt} = -\frac{1}{\tau}(T - T_R). \tag{8}$$

The solution of this equation is

$$T = T_R + (T_0 - T_R) * e^{-t/\tau}, \tag{9}$$

where T_0 is the initial temperature value and τ a constant, which is representative for the temperature changes in this particular spot.

From the computed features for the segmented regions, values for τ can be evaluated using the method of the

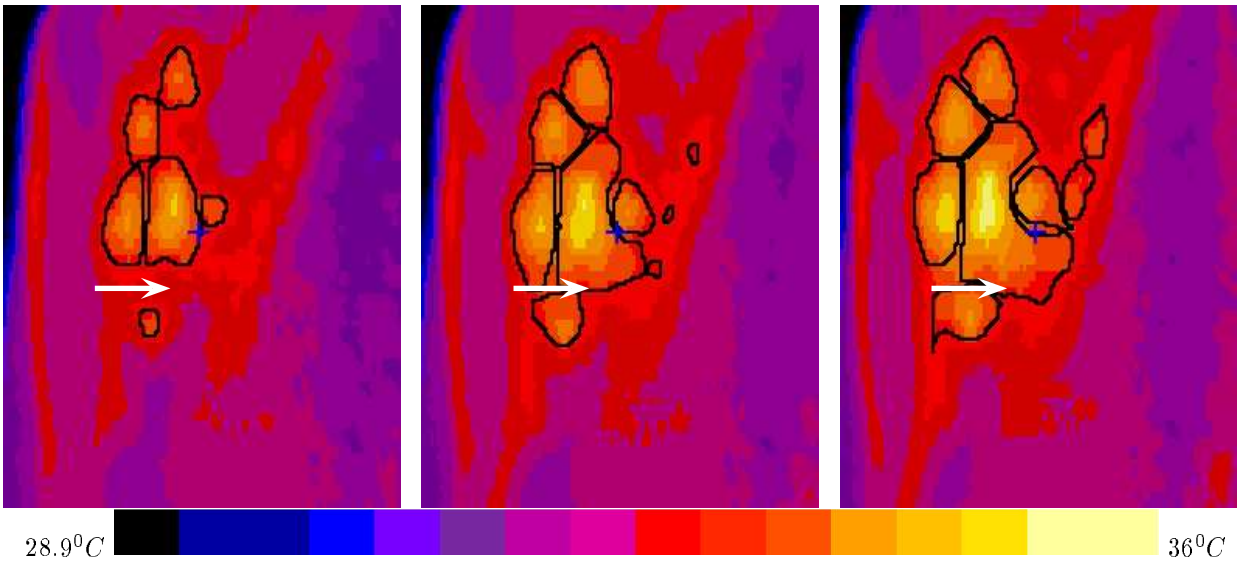

Figure 11: Warming reaction of the skin of the volar forearm after intracutaneous injection of histamine (10 μl, 0.1 %). The arrow marks the injection site. Left: 2 min. after application; middle: 4 min. after stimulus; right: 6 min. after application. The reaction immediately started after the application at different locations which clearly could be separated with the watershed transform. (Parameters for the segmentation: inflammation threshold: 33.32°C, watershed transform-algorithm: $p_m = 51\%$)

minimum square root error. In Figure 12 experimental results are compared to the ideal values of the underlying model for temperature change. Furthermore, it could be seen (Figure 13) that the values for τ are much smaller next to the injection site. Measurements for three locations are shown in Figure 13.

Apparently the geometry of local warming spots reflects the geometry of the underlying network of arterioles which will be dilatated by neurogenic and non neurogenic mechanisms. These spots may correspond to the increased blood flow in preterminal arterioles.

In contrast the visible flare (Figure 14, left) was more uniform and probably due to either vasodilatation in terminal arterioles or in venoles. To analyze the visible flare a 24 Bit CCD Camera has been used for recording. The reddening of the skin could be well segmented using color segmentation by Nischik,[17] even if this is not obvious from the gray level print in Figure 14, left. Since the cameras for visible and thermographic irradiation are at different locations, the detected contour in Figure 14 (left) has to be geometrically distorted to be mapped on Figure 14 (middle).

Superimposing the segmentation results of both methods, we point out that exactly those areas having smaller values of τ lie within the area of the visible flare. Thus, it might be that the spots are exactly those junctions of arterioles which are opened to feed the visible flare. Although the neurogenic character of the flare reaction to histamine is well established the exact nature of the reaction is still unknown. A specific model designed for the reheat of the volar forearm under laboratory conditions was developed by Wilson.[25] This model for interpretation could be adapted to our problem.

A dedicated computer program (Spot–Explorer) has been developed to process thermal images and to quantify the reaction after histamine injection.[8] This program runs under Windows^R and is written in C++.

The implementation of the watershed transform described in Sect. 4 was used in this program. The same algorithm was integrated into Khoros[21] and into an object–oriented programming system in C++ ΐππος.[18,20]

Computation times on a Unix workstation HP 735/99 for a typical image of size 128×155 are approximately 0.05 seconds.

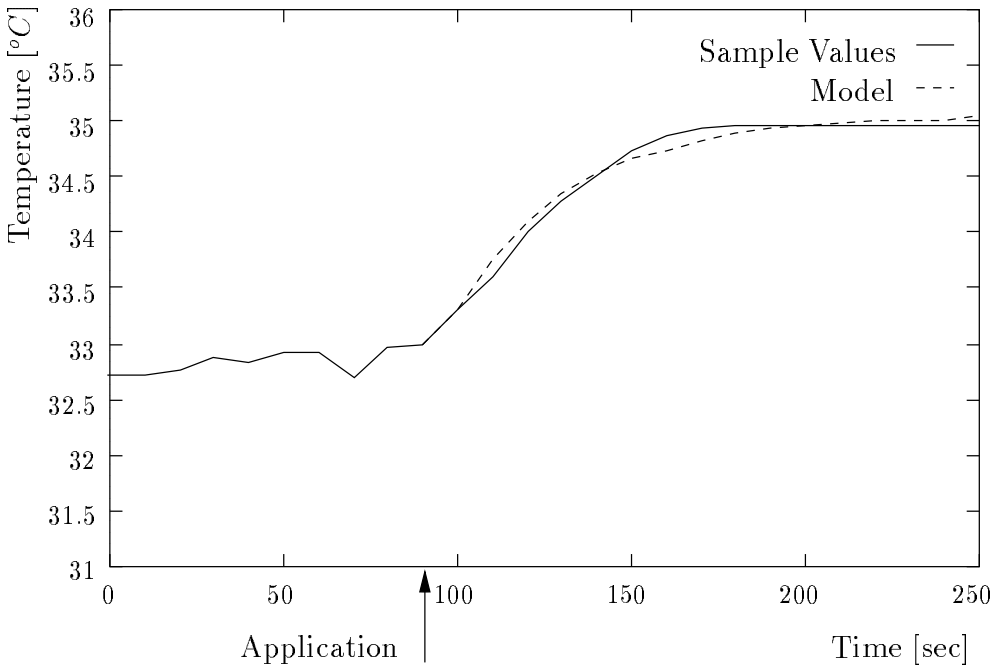

Figure 12: Development of an inflammation as a function of time after histamine injection (sample values and model).

7 CONCLUSION

We presented enhancements to the watershed transform which eliminate some of the deficiencies of other implementations. Using so modified watershed transform we analyse thermographic images of the forearm's skin and present a physiologial interpretation.

The isotherms with some limits (Figure 2) as well as the watershed transform (Figure 11) could be shown to be appropriate methods to process the ongoing of an experimentally induced local inflammation. We showed how the watershed transform can subdivide an image according to the local maxima without any regards to certain thresholds. The inflammation focuses could be clearly separated and traced through the image sequence.

Features of regions segmented by the watershed transform are used to interpret a series of themographic images.

More than 500 images resulting from more than 10 image series have been successfully segmented and evaluated by medical specialists. In order to get results for statistical analysis, more data will be processed and an automatic tracking of region changes is being implemented.

We hope that still uncertain physiological models for the heat distribution under the skin as a function of time can be verified using our new system.

8 REFERENCES

[1] G. A. Baxes. *Digital image processing.* Wiley, New York, 1994.

[2] S. Beucher. Watersheds of funktions and picture segmentation. *Proceedings IEEE International Conference on Acoustic Speech Signal Processing 82*, pages 1928–1931, Mai 1982.

[3] A.N. Bruce. Vaso–dilatator axon–reflexs. *Quarterly Journal of Experimental Physiologiy*, 6:339–354, 1913.

[4] L. A. Chah. Antidromic vasodilatation and neurogenic inflammation. *Pharmacology and Therapeutics*,

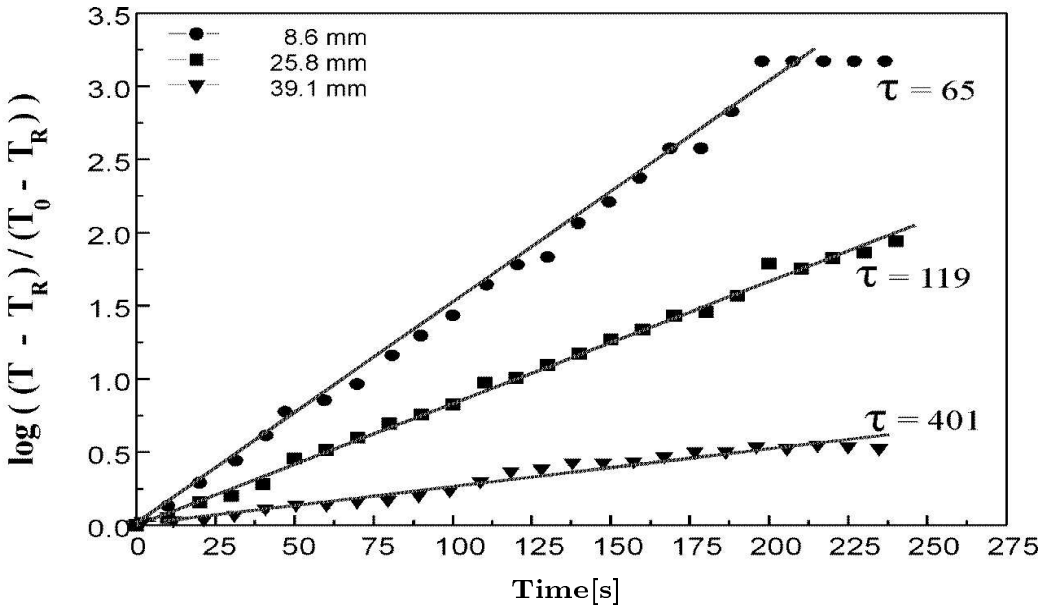

Figure 13: Temperature change at three different locations; the distance to the injection site is shown on the upper left.

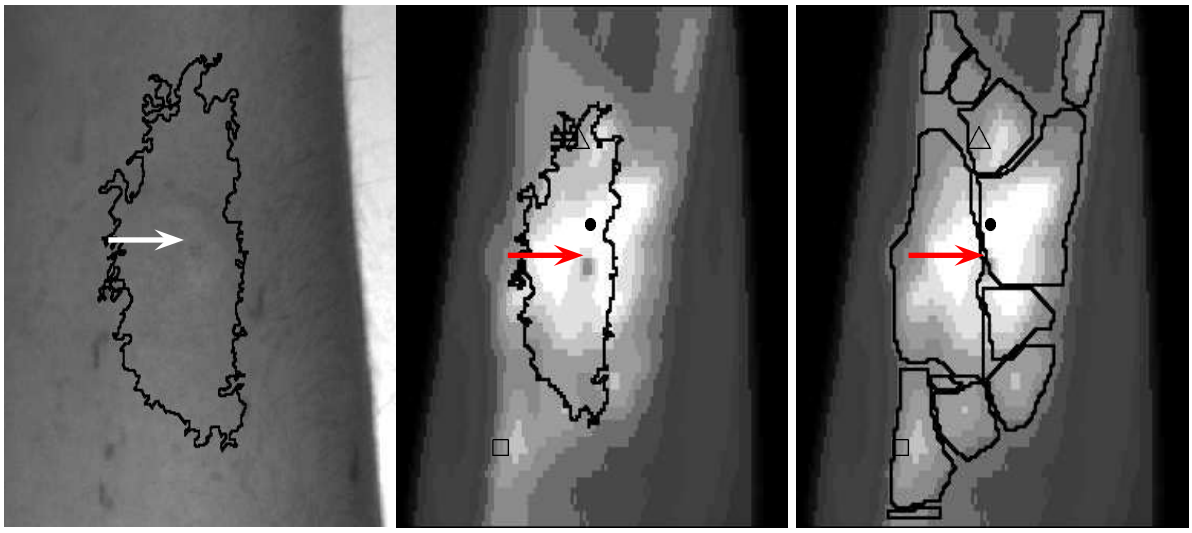

Figure 14: Visual flare with overlayed contour of detected reddening (color image printed as gray level image, left), segmentation of visual flare superimposed to thermographic image (middle). The symbols in the middle image mark the locations for the measurements in Figure 13. The arrow marks the injection site. Thermographic image segmented by watershed transform, (right).

37:275–300, 1988.

[5] H. Digabel and C. Lantuéjoul. Iterative algorithms. *Proc. 2^{nd} European Symp. Quantitative Analysis of Microstructures in Material Science, Biology and Medicine*, pages 85–99, 1978.

[6] B. P. Dobrin, T. J. Viero, and M. Gabbouj. Fast watershed algorithms: analysis and extensions. In *Electronic Image Science and Technology*, pages 209–220, San Jose, CA, 1994. SPIE Proceedings 2180.

[7] F. Friedlander. A sequential algorithm for detecting watersheds on a gray level image. *Proc. 7^{th} Int. Cong. for Stereology*, 6(3):663–668, September 1987.

[8] T. Greiner. Quantitative Analyse neurogener vaskulärer Hautreaktionen in Thermographiebildfolgen (Arbeitstitel). Dissertation am Institut für Physiologie und Experimentelle Pathophysiologie, Erlangen, 1995. in prepration.

[9] M. W. Hanson and W. I. Higgins. Watershed–driven relaxation labeling for image segmentation. In ICIP 94 [see Ref. 11], pages 460–465.

[10] M. Harbeck. Operatorklassen (Arbeitstitel). Dissertation, Technische Fakultät, Universität Erlangen–Nürnberg, Erlangen, in preparation, 1995.

[11] *Proceedings of the International Conference on Image Processing (ICIP)*, Austin, TX, USA, November 1994. IEEE Computer Society Press.

[12] Chr. Knüvener. Implementierung der Wasserscheidentransformation für Thermographiebilder. Studienarbeit, Lehrstuhl für Mustererkennung (Informatik 5), Universität Erlangen–Nürnberg, Erlangen, 1995.

[13] T. Lewis. The nocifensor system of nerves and its reaction. *British Medical Journal*, 194:431–435, 491–494, 1937.

[14] F. Meyer. Skeletons and perceptual graphs. *Signal Processing*, 16:335–363, 1989.

[15] H. Niemann. *Methoden der Mustererkennung.* Akademische Verlagsgesellschaft, Frankfurt, 1974.

[16] H. Niemann. *Pattern Analysis and Understanding.* Springer, Heidelberg, 1990.

[17] M. Nischik, C. Forster, and H.O. Handwerker. Analysis of vascular skin reactions using superimposed video and thermal images. In K. Ammer and E.F.J. Ring, editors, *Thermal imaging in medicine and biology.* Wien, 1995. 6^th Congress of th European Association of Thermology.

[18] D. Paulus. *Objektorientierte und wissensbasierte Bildverarbeitung.* Vieweg, Braunschweig, 1992.

[19] D. Paulus, T. Greiner, and Chr. Knüvener. Wasserscheidentransformation für Thermographiebilder. *DAGM*, 1995. submitted for publication.

[20] D. Paulus and J. Hornegger. *Pattern Recognition and Image Processing in C++.* Advanced Studies in Computer Science. Vieweg, Braunschweig, 1995.

[21] J. R. Rasure and M. Young. Open environment for image processing and software development. In R. B. Arps and W. K. Pratt, editors, *Image Processing and Interchange: Implementation and Systems*, pages 300–310, San Jose, CA, 1992. SPIE Proceedings 1659.

[22] K. Saarinen. Color image segmentation by a watershed algorithm and region adjacency graph processing. In ICIP 94 [see Ref. 11], pages 1021–1025.

[23] J. Shen and S. Castan. An optimal linear operator for step edge detection. *Graphical Models and Image Processing*, 54(2):112–133, März 1992.

[24] L. Vincent and P. Soille. Watersheds in Digital Spaces: An Efficient Algorithm Based on Immersion Simulations. *IEEE Transactions on Pattern Analysis and Machine Intelligence (PAMI)*, 15(6):583–598, 1991.

[25] S. B. Wilson and V.A. Spence. A tissue heat transfer modell for relating dynamic skin temperature changes to physiological parameters. *Physisc in Medicine and Biology*, 33(8):895 – 912, 1988.

[26] S. Zehetbauer. Segmentierung und Analyse drei- und vierdimensionaler Ultraschalldatensätze, 1992.

[27] S. Zehetbauer and U. Meyer-Gruhl. Segmentierung and Analyse drei- und vierdimensionaler Ultraschalldatensätze. In *15. DAGM-Symposium*, pages 118–125. Springer Verlag, Berlin Heidelberg New York, 1993.

	Bild	Physiologie
Eigen	[10] [12] [15] [16] [18] [19] [20]	[8] [17]
Fremd	[1] [2] [5] [6] [7] [9] [14] [21] [22] [23] [24] [26] [27]	[3] [4] [13] [25]